ACS APPLIED MATERIALS & INTERFACES

Surfaces, Interfaces, and Applications

High Tunnelling Magnetoresistance in Magnetic Tunnel Junctions with Sub-nm thick Al2O3 Tunnel Barriers Fabricated Using Atomic Layer Deposition

Jagaran Acharya, Ryan Goul, and Judy Z. Wu

ACS Appl. Mater. Interfaces, **Just Accepted Manuscript** • DOI: 10.1021/acsami.0c03428 • Publication Date (Web): 08 Jul 2020

High Tunnelling Magnetoresistance in Magnetic Tunnel Junctions with Sub-nm thick Al_2O_3 Tunnel Barriers Fabricated Using Atomic Layer Deposition

Jagaran Acharya[1], Ryan Goul, and Judy Wu[1]**

[1]*Department of Physics and Astronomy, University of Kansas, Lawrence, Kansas, 66045, USA*

Corresponding Authors

Jagaran Acharya, email: jagaran@ku.edu

Judy Wu, email: jwu@ku.edu

***Keywords**: Atomic layer deposition, ultrathin film, magnetic tunnel junction, tunnelling magnetoresistance, scanning tunnelling spectroscopy.*

ABSTRACT

Pinhole-free and defect-free ultrathin dielectric tunnel barriers (TBs) is a key to obtaining high tunnelling magnetoresistance (TMR) and efficient switching in magnetic tunnel junctions (MTJs). Among others, atomic layer deposition (ALD) provides a unique approach for the fabrication of ultrathin TBs with several advantages including an atomic-scale control on the TB thickness, conformal coating, and low defects density. Motivated by this, this work explores fabrication and characterization of spin-valve Fe/ALD-Al_2O_3/Fe MTJs with ALD-Al_2O_3 TB thickness of 0.55 nm using *in situ* ALD. Remarkably, high TMR values of ~77% and ~ 90% have been obtained respectively at room temperature and at 100 K, which are comparable to the best reported values on MTJs having thermal AlO_x TBs with optimized device structures. *In situ* scanning tunnelling spectroscopy characterization of the ALD-Al_2O_3 TBs has revealed a higher tunnel barrier height (E_b) of 1.33 ± 0.06 *eV*, in contrast to E_b~0.3-0.6 eV for their AlO_x TB counterparts, indicative of significantly lower defect concentration in the former. This first success of the MTJs with sub-nm thick ALD-Al_2O_3 TBs demonstrates the feasibility of *in situ* ALD for fabrication of pinhole-free and low-defect ultrathin TBs for practical applications and the performance could be further improved through device optimization.

INTRODUCTION

Magnetic tunnel junctions (MTJs) formed by sandwiching an ultrathin insulating barrier between two ferromagnetic (FM) electrodes are the subject of an intensive research recently due to their potential applications in spintronics such as non-volatile MRAM and logic devices [1-3]. The figure-of-merit tunnelling magnetoresistance (TMR) of MTJs depends critically on the quality of the insulating tunnel barrier (TB) and the metal-insulator interface becomes more challenging at sub-nm dielectric thickness range. Specifically, the spin tunnelling current decays exponentially with the TB thickness, which means a stronger coherent tunnelling is anticipated at a smaller TB thickness. It should be noted that the presence of defects in the TB can lead to decoherence of the spin tunnelling, not to mention an increased leakage current. Therefore, research and development of sub-nm thick TBs that are pinhole free and defect-free is important to achieving high-performance MTJs.

Physical vapor deposition (PVD), including magnetron sputtering and molecular beam epitaxy, has been widely adopted for MTJ fabrication with both amorphous AlO_x and epitaxial MgO TBs. The former can be obtained via thermal oxidation of ultrathin Al film on FM electrode in air or in oxygen [4-6] to allow controlled oxygen diffusion into the Al to form AlO_x TBs. The best TMR~70 % at room temperature (RT) has been reported on MTJs with thermal AlO_x TBs. The advantage of the thermal AlO_x TBs is in the simplicity of the fabrication process and large-area uniformity due to the amorphous nature of the AlO_x. However, the thermal AlO_x TBs suffers several drawbacks including defects such as oxygen vacancies that are nonuniform through the TB thickness and can lead to soft dielectric breakdown along with high leakage current especially at sub-nm thicknesses [7-9]. The epitaxial MgO TBs, obtained through post annealing of MTJs at ~350-500 ℃, have advantages of enhanced coherent spin current tunnelling, which leads to enhanced

TMR ~200-350 % at RT [10-17]. However, challenges remain in achieving high yield due to presence of defects including grain boundaries and oxygen vacancies in epitaxial MgO TBs, especially when the TB thickness is approaching 1 nm or smaller. It should be pointed out that the defects such as oxygen vacancies in both AlO_x and MgO TBs are common and difficult to avoid in oxides fabricated using PVD process. In addition, grain boundaries can easily form in epitaxial MgO TBs during recrystallization in the post annealing process and can serve as leakage channels in MTJs. To efficiently control the performance of MTJ devices the optimization of FM electrode for its composition, crystallinity and oxidation along with the quality of interface [18-22] is crucial demanding a smooth and conformal TB with better FM-insulator (FM-I) interface [23-24].

Atomic layer deposition (ALD) provides a promising alternative for the fabrication of ultrathin (sub-nm to 1 nm) leak-free and defect-free TBs. Specifically, ALD provides a unique solution to the issues of defects and pinholes [25-26] (such as oxygen vacancies and grain boundaries) associated with PVD TBs, which have hindered achievement of sub-nm thick TBs. First, ALD is a chemical vapor deposition process that relies on well-defined chemical reactions, which occur only at the sample surface via a ligand exchange between monolayers of the precursors [26]. This minimizes the formation of defects such as oxygen vacancies in oxides. Secondly, ALD growth is self-limiting, enabling atomic control of the TB thickness. Thirdly, ALD coating is conformal, [27-28] which is important in obtaining pinhole-free ultrathin TBs over structured surfaces [29]. Finally, ALD is an industrial approach widely used in complementary metal-oxide-semiconductor technology for ultrathin dielectric gates and capacitors and therefore is an industry-compatible, low-cost approach that is promising for the fabrication of sub-nm thick, pinhole-free, and low-defect TBs for MTJs. This has motivated research recently in ALD growth of TBs of Al_2O_3, MgO and HfO_2 for MTJs [30-32]. However, it has been found that the thickness of the TBs obtained using *ex situ* ALD process is typically in the range of 2-5 nm to avoid leakage current. The TMR values reported on the MTJs with the ALD TBs are in the range of 1-20 % at RT, which is anticipated from the large thickness of these TBs [30-34]. The challenge in achieving thinner ALD TBs is primarily associated to the formation of a native oxide interface between FM electrode and the ALD TB due to exposure of the FM electrode to air or other gases in the *ex situ* ALD processes, which is stronger oxygen getter compared to other metal electrode.

In this work, we explore the fabrication of ALD-Al_2O_3 TBs using an *in situ* ALD process developed recently in our lab [35-37]. MTJs based on a simple Fe/ALD Al_2O_3/Fe structure was employed as a proof of concept in this study and the ALD-Al_2O_3 TB thickness was selected to be 0.55 nm. In order to probe the nucleation effect of the ALD-Al_2O_3 TBs, two sets of devices were compared: one with and the other without a 1 nm thick Al wetting layer on the bottom Fe electrode using both *in situ* scanning tunnelling spectroscopy (STS) and *ex situ* transport measurement. Remarkably, TMR of 77% was demonstrated on Fe/ALD-Al_2O_3/Fe MTJs with an ALD-Al_2O_3 TB of 0.55 nm in thickness. In the following, we will report our experimental results to successfully demonstrate fabrication of Fe/ALD-Al_2O_3/Fe MTJs with 0.55 nm ALD-Al_2O_3 TBs for potential application in future MRAM devices [4-5, 10-12].

EXPERIMENTAL

The MTJs with a multilayer architecture of Nb (50 nm)/Fe (50 nm)/Al (1-0 nm)/ALD-Al_2O_3/Fe (5 nm)/Nb (50 nm) were *in situ* fabricated using an in-house integrated ultra-high vacuum sputtering and ALD chambers. Nb, Fe and Al were DC magnetron sputtered onto a Si/SiO_2 substrate with the deposition rate of 1.7 nm/s, 1.0 nm/s and 0.5 nm/s, respectively, at a base pressure better than $1.0x10^{-7}$ Torr. After sputtering, the samples were transferred *in situ* to the ALD chamber and dynamically heated to the growth temperature of 200 ℃ in the pre-heated ALD chamber. The details of the growth of ALD-Al_2O_3 TBs can be found in our previous work and the optimal processing conditions to minimize interfacial layer (IL) formation have been employed [36]. During the ALD-Al_2O_3 TB growth, a 5 SCCM of N_2 carrier gas was employed together with alternating pulses of H_2O and trimethylaluminum (TMA) precursors, aiming a ligand exchange at the heated sample surface for the formation of the Al_2O_3 [35]. The H_2O and TMA pulse durations were 2 seconds and 1 seconds, respectively. It should be noted that M. Raija *et al* investigated the effect of water pulse duration on the growth rate of ALD-Al_2O_3 film of ~ 200 nm in thickness and found that the ALD-Al_2O_3 growth rate increases with the increasing water pulse duration in the low duration range, followed with a saturation at ~ 0.11-0.12 nm/cycle when the H_2O pulse duration reaches 2-2.5 seconds or longer [38]. In our ALD-Al_2O_3 growth, the H_2O pulse duration of 2 seconds was selected to minimize run-to-run variation of the TB thickness and our calibration of the ALD-Al_2O_3 growth rate, using both ellipsometry on ALD-Al_2O_3 film/Si substrates and capacitors of Al/ALD-Al_2O_3/Al confirmed the ALD-Al_2O_3 growth rate ~ 0.11-0.12 nm/cycle with the details of two methods reported previously [39-41]. This means that the thickness of the 5 cycle ALD-Al_2O_3 TBs in this work is in the range of 0.55-0.60 nm (the nominal thickness of TB has been used throughout the manuscript unless otherwise indicated). Between the pulses of the H_2O and TMA, a purge of the ALD chamber with high-purity N_2 was carried out for 30 seconds [26]. The magnetic properties of these samples, such as magnetization vs magnetic field (M-H) loops with H in the plane of the films, were characterized using a vibrating sample magnetometer (VSM MicroSense, EZ7). Based on the saturated magnetic moments and coercive field estimates from the M-H loop of magnetic thin film structure the choice of free and fixed layers were selected as Fe (50 nm) and Fe (5 nm) respectively. Atomic force microscopy (AFM, WiTec Alpha 300) in contact mode was used to characterize topography of the samples and surface roughness (R_a) was calculated using root-mean square average of roughness within in the scan area. *In situ* STS spectra were obtained to investigate the electronic properties of TBs on 5 cycles of ALD-Al_2O_3/Fe (20 nm) structure referred to as a half-cell without and with an Al (1 nm) wetting layer. Specifically, *dI/dV* spectra were collected simultaneously using a lock-in amplifier with a voltage modulation of 30 mV at 5 kHz, with a set-point bias of 2.0 V and current ~ 200 pA to assure the STS tip would not crash. The conduction band minimum, denoted as tunnel barrier height (E_b), was estimated by the intersection of two bisquare-method linear fits to ln(*dI/dV*) similar to the method previously reported [42]. One line fits the band gap regime, and the other the conduction band since in log scale, these two regions are roughly linear. This ln(*dI/dV*) linear fit method was chosen over *I-V* or *(dI/dV)/(I/V)* fit methods for its insensitivity to the noise in the STS spectra [43-44]. MTJs were fabricated using photolithograph/electron-beam lithography and ion milling. Two sets of MTJ devices were fabricated in this work; both have 5 cycle ALD-Al_2O_3 TBs (thickness 0.55-0.60 nm). One set of the MTJs has a 1 nm thick Al wetting layer on the bottom Fe electrode, i.e. Nb (50 nm)/Fe (5 nm)/Al (1nm)/ ALD-Al_2O_3 0.55nm /Fe (50 nm)/Nb (50 nm) while the other, has no such a wetting layer: Nb (50 nm)/Fe (5 nm)/ ALD-Al_2O_3 0.55 nm/Fe (50 nm). The Al wetting layer was introduced for a comparison of the quality of the ALD Al_2O_3 TBs on Fe with respect to on Al. In our previous studies, Al has been found favourable by providing a dense layer of the OH-groups during the first H_2O pulse of the ALD-Al_2O_3 TB growth, which is key to minimizing the defective IL and hence the defect concentration in the ALD-Al_2O_3 TBs. It should be realized that the formation of a dense OH-group layer may be hindered on other metals including ferromagnetic metal electrodes [36]. By inclusion of an ultrathin Al wetting layer to alter the electrode surface chemistry, and compare with the samples without such a wetting layer, the effect of such a wetting layer on the ALD-Al_2O_3 TB quality and the TMR of the device can be evaluated. A slightly lower

E_b ~ 1.31 eV on ALD Al_2O_3 TB was revealed on Fe electrode as compared to E_b ~ 1.47 eV with the 1 nm Al wetting layer, suggesting comparable quality ALD Al_2O_3 TBs can be achieved without the 1 nm Al wetting layer. MTJs were obtained, current-voltage characteristics were collected using the four-probe measurement. The noise was controlled below 10 nV after wiring through optimization of the contact resistance. The resistance-area (*RA*) product was measured to examine the uniformity of MTJ devices as function of the ALD-Al_2O_3 TB thickness. Since an exponential dependence of the *RA* on the TB thickness is anticipated, the *RA* data was fitted accordingly to extract the ALD-Al_2O_3 TB height. For simplicity, a spin valve structured MTJ was employed in this work. The TMR measurement was performed in a physical property measurement system (PPMS, Quantum Design Evercool II). The tunnelling resistance of MTJs in parallel (R_P) and anti-parallel (R_{AP}) configurations were obtained. The figure-of-merit TMR is estimated based on the relative change in percentage between R_P and R_{AP} configuration as TMR $= \frac{R_{AP} - R_P}{R_P} \times 100\ \%$.

RESULTS AND DISCUSSIONS

Figure 1(a) show the M-H loops measured on several samples including Fe (50 nm), Fe (50 nm)/Al (7 nm), Nb (50 nm)/Fe (50 nm) and Nb (50 nm)/Fe (50 nm)/Al (7 nm) fabricated using *in situ* DC sputtering. An overall improvement in saturated magnetization of the multilayered samples as compared to the single-layered Fe ones is most probably due to the prevention of Fe from oxidation to form non-magnetic FeO_x by the capping layers of Nb or/and Al. Based on the literature, negligible intermetallic formation between Nb/Fe or Fe/Al structure is anticipated [45-46]. Since Al is not ferromagnetic and the paramagnetic moment for the very thin (7 nm) Al layer, as opposed to that from the 50 nm of ferromagnetic Fe layer, is negligible, the comparable M-H loops for the Nb (50 nm)/Fe (50 nm) and Nb (50 nm)/Fe (50 nm)/Al (7 nm) samples are anticipated. Figure 1(b) show the M-H loops of two each of 50 nm (black and red) and 5 nm (purple and blue) thick Fe films and the overlap of the M-H loops for the samples of the same thickness illustrates reliable reproducibility from run to run. Based on the M-H loops, the coercive field of about 52 Oersted and 20 Oersted, respectively, can be estimated for the 50 nm and 5 nm thick Fe films. Thus, thicker Fe film serves as the fixed layer while the thinner one, the free layer in the MTJs of this work.

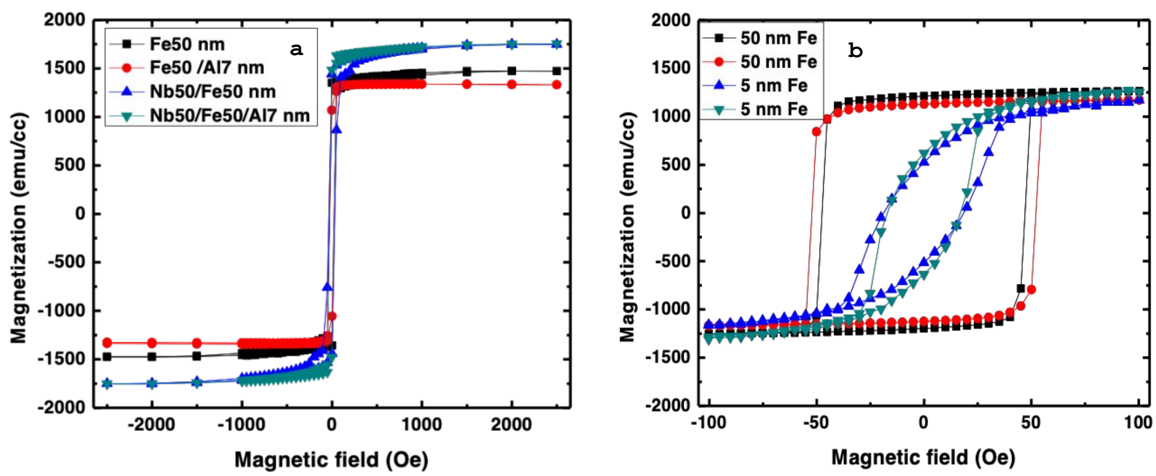

Figure 1. Magnetization vs magnetic field (M-H) loop for multi-layered structure with a) Fe (50 nm), Fe (50 nm)/Al (7 nm), Nb (50 nm)/Fe (50 nm) and Nb (50 nm)/Fe (50 nm)/Al (7 nm) b) M-H loop for

Figure 2 exhibits representative AFM images taken on three thin film samples: Fe (50 nm), Nb (50 nm)/Fe (50 nm), and Nb (50 nm)/Fe (50 nm)/Al (7 nm). Overall, all three samples have very smooth surface that are featureless over the AFM scan area of 5x5 μm^2. In fact, the similar AFM scans were performed on different locations of these samples to ensure uniformity. The surface roughness (R_a) calculated based on the AFM images are 0.90 nm, 0.85 nm and 0.82 nm, respectively, on the Fe (50 nm), Nb (50 nm)/Fe (50 nm), and Nb (50 nm)/Fe (50 nm)/Al (7 nm) samples. The low R_a values on each of the three layers of the bottom electrode for the MTJs has confirmed an ideal smooth surface of the metal electrode for growth of the ALD-Al_2O_3 TBs. It should be mentioned that these R_a values are consistent with that measured in our previous study of surface morphology of samples before and after the ALD-Al_2O_3 TB growth[29, 47]. In particular, a comparable and slightly improved R_a after the ALD-Al_2O_3 TB growth is anticipated from the conformal coating of the ALD.

Figure 3 shows schematically the two device structures of the MTJs investigated in this work: one with (Figure 3(a)), and the other, without (Figure 3(b)) a 1 nm thick Al wetting layer on top of the bottom Fe electrode. The Al wetting layer has been found to allow better nucleation of the ALD-Al_2O_3 TBs with a negligible defective metal-insulator interface [36]. Considering ALD is a chemical process, the improved nucleation of the ALD-Al_2O_3 TBs on the metal surface can lead to improved TB quality, especially the defect concentration that affects the ALD-Al_2O_3 TB's height, and dielectric breakdown [35]. However, the presence of a non-ferromagnetic layer of Al between the two ferromagnetic Fe electrodes is undesirable since it reduces the coherent spin tunnelling through the MTJ. Therefore, the Al wetting layer thickness was controlled to be around 1 nm for a comparison of the MTJ performance of with and without such a wetting layer.

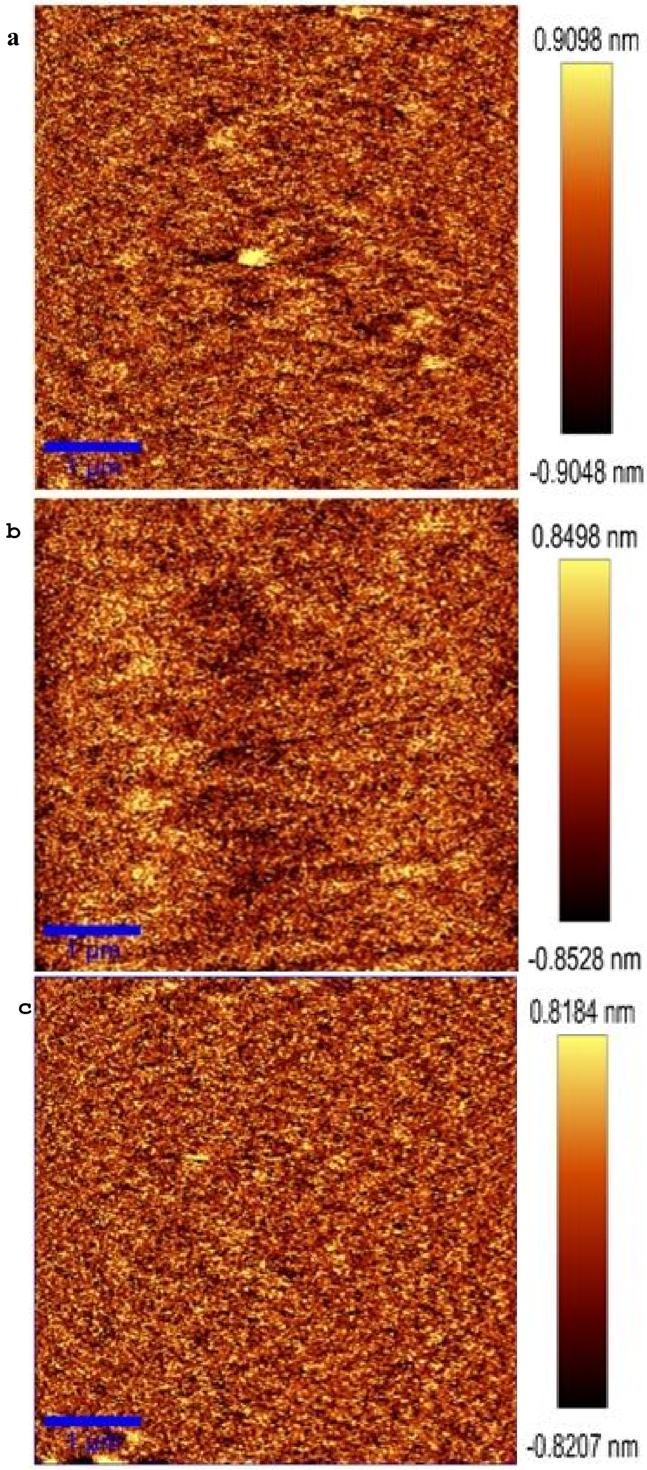

Figure 2. AFM images of a) Fe (50 nm), b) Nb (50 nm)/Fe (50 nm), and c) Nb (50 nm)/Fe (50 nm)/Al (7 nm) thin films deposited on SiO_2.

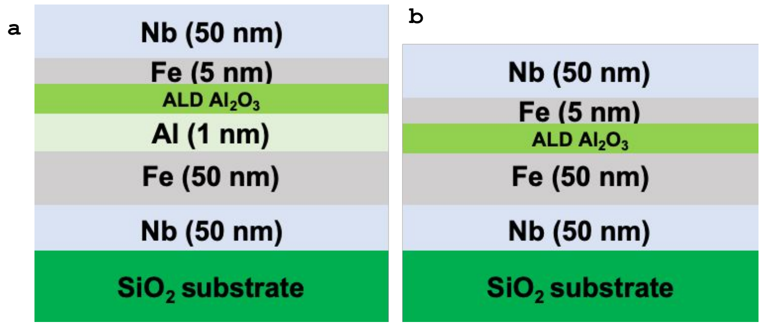

Figure 3. Schematic of the device structures of MTJs investigated in this work a) with 1 nm Al wetting layer and b) without Al wetting layer on the bottom Fe electrode.

Figure 4 compares a representative STS *dI/dV* spectra taken on 5 cycles (or 0.55 nm thick) ALD-Al_2O_3 TBs with (Figure 4(a)) and without (Figure 4(b)) the 1 nm thick Al wetting layer on Fe bottom electrode, or the half cells of the two kinds of MTJs shown in Figure 3. The *dI/dV* spectra on the two devices show qualitatively similar characteristics of a dielectric TB, indicating that the ALD-Al_2O_3 TBs can form on both surfaces of the Al and Fe. However, quantitative differences are clearly visible especially in values of the E_b's. Specifically, the $E_b \sim 1.40 \pm 0.16\ eV$ (overall average $1.47 \pm 0.05\ eV$) observed on the ALD-Al_2O_3 TB with the Al wetting layer in Figure 4(a) is higher than the $E_b \sim 1.33 \pm 0.06\ eV$ (overall average $1.31 \pm 0.03\ eV$) of Al_2O_3 grown directly on Fe (Figure 4(b)), indicating a higher defect concentration in the latter [35, 37]. This may be attributed to the formation of an IL of FeO_x between the Fe and ALD-Al_2O_3 TBs due to the less dense Fe atoms on the surface of the Fe as compared to the Al atom density on the Al surface [36]. The larger inter-atom distance on the Fe surface as compared to the Al surface would lead to more difficult hydroxylation of the Fe surface during the first H_2O pulse of the ALD-Al_2O_3 growth. When a partial decomposition of the H_2O to oxygen and hydrogen occurs, instead of to hydroxyl groups (OH^{-1}) on the metal surface, formation of defective FeO_x IL may form. The ultrathin ALD-Al_2O_3 TBs grown on the defective native oxide IL would be defective, which explains the reduced E_b of the ALD-Al_2O_3 TB on Fe as compared to that on Al. Nevertheless, the average $E_b \sim 1.31 \pm 0.03\ eV$ on the ALD-Al_2O_3 TBs of 0.55 nm in thickness on Fe is only 12% lower than that on Al.

This means the effect of the FeO_x IL is insignificant. In addition, the $E_b \sim 1.31 \pm 0.03$ eV eV of the 0.55 nm thick ALD-Al_2O_3 TB on Fe is significantly better than the low $E_b \sim$ 0.3- 0.6 eV for thermal TB based devices [5, 8, 48]. This suggests that the defect concentration in ALD-Al_2O_3 TBs is much reduced as compared to the thermal AlO_x TB case. This argument is supported by the significantly lower leakage current and harder dielectric breakdown observed in the former in contrast to the latter [35, 37].

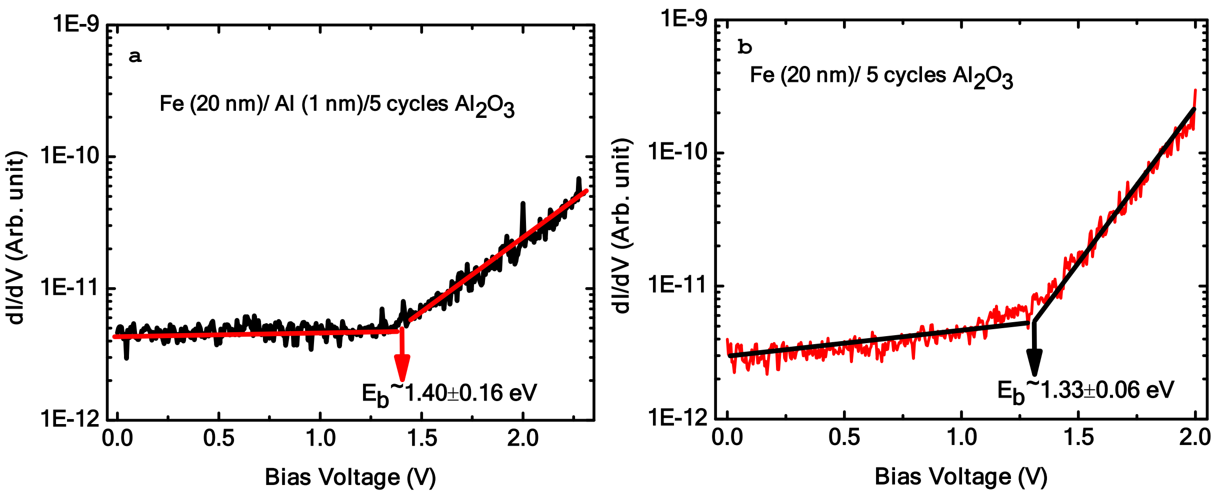

Figure 4. STS *dI/dV* spectra taken on the ALD-Al_2O_3 TBs a) with 1 nm Al wetting layer and b) without Al wetting layer on Fe bottom electrode. The thickness of the ALD-Al_2O_3 TB is 0.55 nm made with 5 ALD cycles.

Figure 5 shows the RA vs. H hysteresis loops measured at 100 K and 300 K on the two representative Nb/Fe (50 nm)/ALD-Al_2O_3/Fe (5 nm)/Nb MTJs with an 1 nm thick Al wetting layer (Figures 5(a)-(b)) and without (Figures 5(c)-(d)), respectively, at 300 K (RT) and 100 K. The observed hysteretic behaviour on both samples is anticipated for MTJs due to the switching of the magnetic moments in the free Fe layer (top Fe electrode) between parallel to anti-parallel orientations with respect to that in the pinned Fe layer (bottom Fe electrode) as the applied H field exceeds the coercive field of the free layer. The TMR values can be calculated from the RA-H loops (see Experimental) are 4.2 % and 4.3 % at 300 K and 100 K, respectively, for the MTJ with the 1 nm thick Al wetting layer. These low TMR values indicate that the presence of the non-ferromagnetic Al wetting layer, even only at the 1 nm thickness, between the two Fe electrodes is undesirable since it behaves like a barrier that could significantly reduce the coherent spin tunnelling. When the Al wetting layer is removed, significantly higher TMR ~77 % at 300 K and ~90 % at 100 K, respectively, are obtained on the counterpart MTJ without Al wetting layer as shown in Figures 5(c)-(d). The current state-of-the art MTJs with optimized FM electrode $Co_{60}Fe_{20}B_{20}$, pinning layer IrMn, optimized AlO_x TBs formed by oxidizing 1 nm Al in plasma of Ar/O_2 and magnetic thermal annealing at 265℃ for 1 hour to achieve better FM-I interface demonstrates the maximum TMR ~70 % at RT [4-6]. An improved TMR~81.3% at RT (and ~95 % at 100 K) was reported by further optimization of the AlO_x TBs using inductively coupled plasma oxidation on $Co_{40}Fe_{40}B_{20}$ electrodes [49]. Therefore, the TMR values obtained in the MTJs with ALD-Al_2O_3 TBs of 0.55 nm in thickness are comparable to the best so far achieved in MTJs made with PVD approaches. The trend of increasing TMR values with decreasing operation temperatures is anticipated from reduced scattering effect by phonons and magnons at lower temperatures [50-51]. In fact, the 17% increase in the TMR value at 100 K as from that at 300 K in the MTJs with the 0.55 nm ALD-Al_2O_3 TB is comparable to that previously reported on MTJs [49]. Interestingly, the two types of MTJ devices shown in Figure 5 exhibit very different RA values. Without the Al wetting layer, the RA values measured in multiple MTJ devices are in the range of 862±120 Ω.µm² for junction areas of 100, 75 and 25 µm² at RT, which is consistent with RA shown in Figures 5(c)-(d). In contrast, larger RA values by 1-2 order of magnitude higher are observed on MTJs with the Al wetting layer. Considering the similar STS dI/dV spectra and E_b values for the ALD-Al_2O_3 TBs grown on Fe without and with the 1 nm Al wetting layer (Figure 4), the Al wetting layer may be intact up when the ALD-Al_2O_3 TB growth is completed. Therefore, the significantly higher RA values in the MTJs with the Al wetting layer, especially as compared to that reported in literature, [52-53] may be attributed to the oxidation of the Al wetting layer during the post fabrication processes for both top electrode fabrication after the ALD-Al_2O_3 TB growth and the MTJ device fabrication including multiple steps of photolithography, e-beam lithography, ion milling, liftoff and deposition. This means the practical TB thickness is much thicker than 0.55-0.60 nm in the Fe/Al/ALD-Al_2O_3/Fe MTJs shown in Figures 5(a)-(b). This result hence suggests that the Al wetting layer is not necessary in the Fe/Al/ALD-Al_2O_3/Fe MTJs and may even cause issues of post oxidation, resulting in degraded MTJ performance.

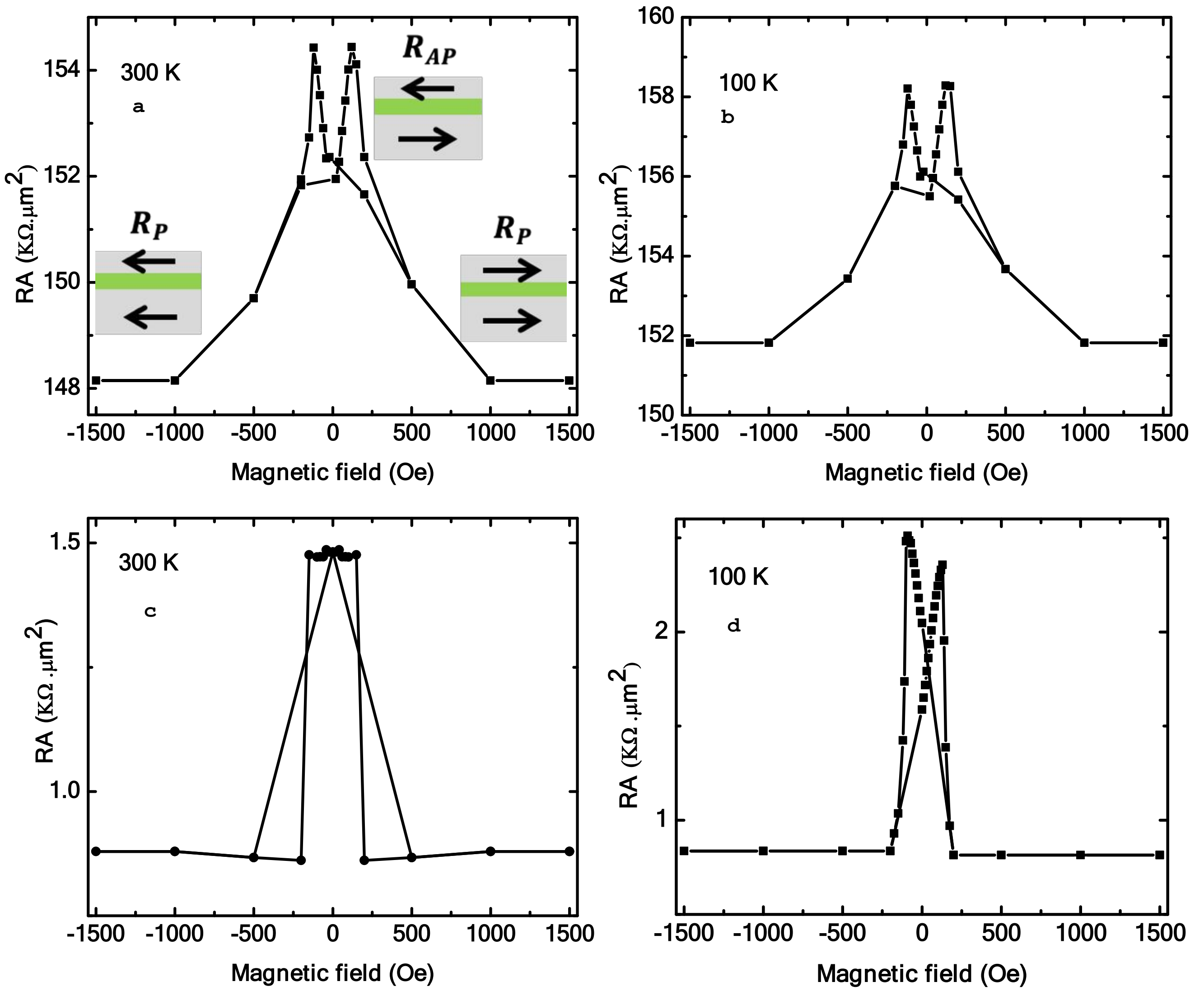

Figure 5. Hysteresis loops of RA vs magnetic field for a representative MTJ of Nb /Fe (50 nm)/Al (1-0 nm)/ALD-Al_2O_3/Fe (5 nm)/Nb with a 1 nm thick Al wetting layer at (a) at 300 K and (b) 100 K respectively; and for its counterpart without the Al wetting

The current state-of-art MTJ fabrication uses optimized FM electrode, antiferromagnetic pinning layer, and magnetic thermal annealing and the best figure-of-merit TMR is in the range of 10-70 % for MTJs with AlO_x TBs [1-6, 49] and 200-350 % for MTJs having epitaxial MgO TBs [10-15]. However, further reduction of these TBs to sub-nm thickness range remains challenging due to defects, such as grain boundaries and oxygen vacancies, within the dielectric TBs, resulting in increased leakage current and incoherent tunnelling in both AlO_x or MgO based MTJs [7-9, 54-61].This is in agreement with the observed reduced E_b in range of 0.3- 0.6 eV for thermal TB based devices [5, 8, 48].

While this work represents the first success in fabrication of MTJs with sub-nm thick ALD-Al_2O_3 TBs, many efforts have been put in the synthesis of ALD TBs for MTJs in the past [30-34]. The reported thickness of the ALD TBs is typically in the range 2-5 nm due to significant increase in leakage at smaller TB thicknesses [30-31, 33-34]. One of the primary reasons leading to the difficulties in achieving thinner, leak-free ALD TBs in the prior effort is that these ALD TBs were fabricated using *ex situ* processes. Thus, exposure of metal surfaces to an ambient condition before ALD TB growth implies that a native oxide IL forms before nucleation of the ALD TB [30-31, 33-34, 62-64]. The IL has a significant impact on the quality of the ALD TBs growth on top of it because it is typically defective with oxygen vacancies and pinholes leading to the defective growth continue to ALD TBs, which explains the significant increase in leakage with *ex situ* ALD TBs at thickness below 2-5 nm [7-9]. However, the control over the formation of a native oxide IL, which can even form in an *in situ* ALD process have been optimized in our previous work [35, 37]. The defective ALD TBs obtained in *ex situ* ALD processes is illustrated in the low E_b together with soft dielectric breakdown. In the *in situ* ALD processes, the IL can be reduced to negligible level ~ 0.1-0.2 $A°$ [39], which not only enables sub-nm think pin-hole free ALD TBs to be achieved, but also reduces the defect concentration in ALD-Al_2O_3 TBs as illustrated in the E_b of 1.31-1.47 eV that is significantly higher than the previously reported E_b~0.3-0.6 eV for AlO_x TBs [5, 8, 48]. This work therefore illustrates the critical importance in controlling the FM/ALD TB interface and the potential of the *in situ* ALD process for fabrication of ultrathin, high quality TBs for MTJs [1-6, 49]. Finally, it is worth mentioning that the ALD-Al_2O_3 TBs are highly uniform as reflected in the negligible TB thickness dependence of E_b values [35-37]. This is in contrast to the strong TB thickness dependence of the tunnel barrier height in the AlO_x TBs obtained via oxygen diffusion into the Al or Al-alloys [65].

CONCLUSIONS

In summary, this work demonstrates the first success in the fabrication and characterization of Fe/ALD-Al_2O_3/Fe MTJs with sub-nm thick ALD-Al_2O_3 TB using a newly developed *in situ* ALD process. Differing fundamentally from the *ex situ* ALD processes, the *in situ* ALD allows a control of the defective native oxide IL at the metal-insulator interface to a negligible level. This enables sub-nm thick, pinhole-free, and low-defect ALD TBs to be achieved on FM metal electrodes, such as Fe, for MTJs. The *in situ* STS study performed on the 0.55 nm thick ALD-Al_2O_3 TBs grown on Fe reveals a significantly higher $E_b \sim 1.33 \pm 0.06\ eV$ that is 4.4-2.2 times higher than that of their thermal AlO_x TB counterparts obtained via oxygen diffusion in to the Al films. Since the reduction of the E_b is attributed to the defect concentration of the dielectric TBs, this enhanced E_b in the ALD-Al_2O_3 TBs confirms the significantly reduced defect concentration in the ALD-Al_2O_3 TBs as compared to their thermal AlO_x TBs counterparts. Remarkably, TMR values of ~77% at 300 K and 90 % at 100 K have been achieved in Fe/ALD-Al_2O_3/Fe MTJs with 0.55 nm thick ALD-Al_2O_3 TBs, which are comparable the best reported on the MTJs with thermal AlO_x TBs and can be further enhanced with optimization of the devices. This result therefore demonstrates the feasibility of the ALD TBs that can potentially meet the requirements of sub-nm thin, pinhole-free and defect-free for applications in spintronics and neuromorphic memory devices.

AUTHOR INFORMATION

Corresponding Authors

*Email: jagaran@ku.edu

*Email: jwu@ku.edu

ORCID

Jagaran Acharya: 0000-0003-1129-0974

Judy Wu: 0000-0001-7040-4420

Author Contributions

J.A. and J.Z.W. designed the experiment. J.A. prepared the samples and performed the measurement and properties characterization with most of the analysis. R. G. contributed with STS sample fabrication and measurement. All authors contributed for the discussion of results. J.A. and J.Z.W. led the effort in the development of the manuscript.

Funding Sources

This research was supported in part by ARO Contract No. ARO-W911NF-16-1-0029 and NSF Contract Nos. NSF- ECCS-1809293, NSF-DMR-1909292, and NSF-DMR-1508494.

Notes

The Authors declare no competing financial interest.

ACKNOWLEDGMENTS

This research was supported in part by ARO Contract No. ARO-W911NF-16-1-0029 and NSF Contract Nos. NSF- ECCS-1809293, NSF-DMR-1909292, and NSF-DMR-1508494.

REFRENCES

1. Žutić, I.; Fabian, J.; Sarma, S. D., Spintronics: Fundamentals and Applications. *Reviews of modern physics* **2004,** *76*, 323.

2. Chappert, C.; Fert, A.; Van Dau, F. N., The Emergence of Spin Electronics in Data Storage. *Nature materials* **2007,** *6*, 813.

3. Hirohata, A.; Takanashi, K., Future Perspectives for Spintronic Devices. *Journal of Physics D: Applied Physics* **2014,** *47*, 193001.

4. Miyazaki, T.; Tezuka, N., Giant Magnetic Tunneling Effect in Fe/Al2o3/Fe Junction. *Journal of Magnetism and Magnetic Materials* **1995,** *139*, L231-L234.

5. Miyazaki, T.; Tezuka, N., Spin Polarized Tunneling in Ferromagnet/Insulator/Ferromagnet Junctions. *Journal of magnetism and magnetic materials* **1995,** *151*, 403-410.

6. Wang, D.; Nordman, C.; Daughton, J. M.; Qian, Z.; Fink, J., 70% Tmr at Room Temperature for Sdt Sandwich Junctions with Cofeb as Free and Reference Layers. *Magnetics, IEEE Transactions on* **2004,** *40*, 2269-2271.

7. Tan, E.; Mather, P.; Perrella, A.; Read, J.; Buhrman, R., Oxygen Stoichiometry and Instability in Aluminum Oxide Tunnel Barrier Layers. *Physical Review B* **2005,** *71*, 161401.

8. Kang, X.; Ying, L.; Wang, H.; Zhang, G.; Peng, W.; Kong, X.; Xie, X.; Wang, Z., Measurements of Tunneling Barrier Thicknesses for Nb/Al–Alox/Nb Tunnel Junctions. *Physica C: Superconductivity* **2014,** *503*, 29-32.

9. Kleinsasser, A. W.; Miller, R. E.; Mallison, W. H., Dependence of Critical Current Density on Oxygen Exposure in Nb-Alo/Sub X/-Nb Tunnel Junctions. *Applied Superconductivity, IEEE Transactions on* **1995,** *5*, 26-30.

10. Yuasa, S.; Nagahama, T.; Fukushima, A.; Suzuki, Y.; Ando, K., Giant Room-Temperature Magnetoresistance in Single-Crystal Fe/Mgo/Fe Magnetic Tunnel Junctions. *Nature materials* **2004,** *3*, 868-871.

11. Xiang, H.; Ji, C.-X.; Yang, J. J.; Chang, Y. A., Compositional Effect of Bcc Co 100− X Fe X Electrodes on Magnetoresistance in Alo X-Based Magnetic Tunnel Junctions. *Applied Physics A: Materials Science & Processing* **2010,** *98*, 707-710.

12. Bowen, M.; Bibes, M.; Barthélémy, A.; Contour, J.-P.; Anane, A.; Lemaıtre, Y.; Fert, A., Nearly Total Spin Polarization in La 2/3 Sr 1/3 Mno 3 from Tunneling Experiments. *Applied Physics Letters* **2003,** *82*, 233-235.

13. Yuasa, S.; Suzuki, Y.; Katayama, T.; Ando, K., Characterization of Growth and Crystallization Processes in Cofeb∕Mgo∕Cofeb Magnetic Tunnel Junction Structure by Reflective High-Energy Electron Diffraction. *Applied Physics Letters* **2005,** *87*, 242503.

14. Ikeda, S.; Hayakawa, J.; Ashizawa, Y.; Lee, Y.; Miura, K.; Hasegawa, H.; Tsunoda, M.; Matsukura, F.; Ohno, H., Tunnel Magnetoresistance of 604% at 300 K by Suppression of Ta Diffusion in Co Fe B∕Mg O∕Co Fe B Pseudo-Spin-Valves Annealed at High Temperature. *Appl. Phys. Lett.* **2008,** *93*, 082508.

15. Hayakawa, J.; Ikeda, S.; Lee, Y. M.; Matsukura, F.; Ohno, H., Effect of High Annealing Temperature on Giant Tunnel Magnetoresistance Ratio of Co Fe B∕Mg O∕Co Fe B Magnetic Tunnel Junctions. *Applied Physics Letters* **2006,** *89*, 232510.

16. Ikeda, S.; Miura, K.; Yamamoto, H.; Mizunuma, K.; Gan, H.; Endo, M.; Kanai, S.; Hayakawa, J.; Matsukura, F.; Ohno, H., A Perpendicular-Anisotropy Cofeb–Mgo Magnetic Tunnel Junction. *Nature materials* **2010,** *9*, 721-724.

17. Wang, M.; Cai, W.; Cao, K.; Zhou, J.; Wrona, J.; Peng, S.; Yang, H.; Wei, J.; Kang, W.; Zhang, Y., Current-Induced Magnetization Switching in Atom-Thick Tungsten Engineered Perpendicular Magnetic Tunnel Junctions with Large Tunnel Magnetoresistance. *Nature communications* **2018,** *9*, 1-7.

18. Moodera, J. S.; Kinder, L. R.; Wong, T. M.; Meservey, R., Large Magnetoresistance at Room Temperature in Ferromagnetic Thin Film Tunnel Junctions. *Physical review letters* **1995,** *74*, 3273.

19. Zhang, Z.-G.; Freitas, P.; Ramos, A.; Barradas, N.; Soares, J., Resistance Decrease in Spin Tunnel Junctions by Control of Natural Oxidation Conditions. *Applied Physics Letters* **2001,** *79*, 2219-2221.

20. Lee, J.; Kim, S.; Yoon, C.; Kim, C.; Park, B.; Lee, T. D., Thermal Stability of the Exchanged Biased Cofe/Irmn Electrode for the Magnetic Tunnel Junction as a Function of Cofe Thickness. *Journal of applied physics* **2002,** *92*, 6241-6244.

21. Yang, J. J.; Ji, C.; Chang, Y. A.; Ke, X.; Rzchowski, M., Over 70% Tunneling Magnetoresistance at Room Temperature for a Cofe and Al O X Based Magnetic Tunnel Junction. *Appl. Phys. Lett.* **2006,** *89*, 202502.

22. Rhee, J. R., Dependence of Magnetic Tunnel Junction Properties on Tunnel Barrier Roughness. *Journal of Magnetism and Magnetic Materials* **2006,** *304*, e300-e302.

23. Diešková, M.; Konôpka, M.; Bokes, P., Atomic and Electronic Structure of Ultra-Thin Al/Alo X/Al Interfaces. *Surface Science* **2007,** *601*, 4134-4137.

24. Gangineni, R.; Bellouard, C.; Duluard, A.; Negulescu, B.; Baraduc, C.; Gaudin, G.; Tiusan, C., Interfacial Electronic Transport Phenomena in Single Crystalline Fe-Mgo-Fe Thin Barrier Junctions. *Applied Physics Letters* **2014,** *104*, 182402.

25. Zhu, C.; Cho, B. J.; Li, M. F., Atomic Layer Deposited High-K Films and Their Role in Metal-Insulator-Metal Capacitors for Si Rf/Analog Integrated Circuit Applications. *Chemical Vapor Deposition* **2006,** *12*, 165-171.

26. George, S. M., Atomic Layer Deposition: An Overview. *Chemical Reviews* **2009,** *110*, 111-131.

27. Banerjee, P.; Perez, I.; Henn-Lecordier, L.; Lee, S. B.; Rubloff, G. W., Nanotubular Metal–Insulator–Metal Capacitor Arrays for Energy Storage. *Nature Nanotechnology* **2009,** *4*, 292-296.

28. Malek, G. A.; Brown, E.; Klankowski, S. A.; Liu, J.; Elliot, A. J.; Lu, R.; Li, J.; Wu, J., Atomic Layer Deposition of Al-Doped Zno/Al2o3 Double Layers on Vertically Aligned Carbon Nanofiber Arrays. *ACS applied materials & interfaces* **2014,** *6*, 6865-6871.

29. Goul, R.; Wilt, J.; Acharya, J.; Liu, B.; Ewing, D.; Casper, M.; Stramel, A.; Elliot, A.; Wu, J. Z., Electron Tunneling Properties of Al2o3 Tunnel Barrier Made Using Atomic Layer Deposition in Multilayer Devices. *AIP Advances* **2019,** *9*, 025018.

30. Liu, X.; Shi, J., Magnetic Tunnel Junctions with Al2o3 Tunnel Barriers Prepared by Atomic Layer Deposition. *Applied Physics Letters* **2013,** *102*, 202401.

31. Fabretti, S.; Zierold, R.; Nielsch, K.; Voigt, C.; Ronning, C.; Peretzki, P.; Seibt, M.; Thomas, A., Temperature and Bias-Voltage Dependence of Atomic-Layer-Deposited Hfo2-Based Magnetic Tunnel Junctions. *Applied Physics Letters* **2014,** *105*, 132405.

32. Mantovan, R.; Vangelista, S.; Kutrzeba-Kotowska, B.; Cocco, S.; Lamperti, A.; Tallarida, G.; Mameli, D.; Fanciulli, M., Synthesis of Magnetic Tunnel Junctions with Full in Situ Atomic Layer and Chemical Vapor Deposition Processes. *Thin solid films* **2012,** *520*, 4820-4822.

33. Vangelista, S.; Mantovan, R.; Cocco, S.; Lamperti, A.; Salicio, O.; Fanciulli, M., Chemical Vapor Deposition Growth of Fe3o4 Thin Films and Fe/Fe3o4 Bi-Layers for Their Integration in Magnetic Tunnel Junctions. *Thin solid films* **2012,** *520*, 4617-4621.

34. Mantovan, R.; Vangelista, S.; Kutrzeba-Kotowska, B.; Lamperti, A.; Manca, N.; Pellegrino, L.; Fanciulli, M., Fe3− Δo4/Mgo/Co Magnetic Tunnel Junctions Synthesized by Full in Situ Atomic Layer and Chemical Vapour Deposition. *Journal of Physics D: Applied Physics* **2014,** *47*, 102002.

35. Wilt, J., Gong, Sakidja, R., Goul, R.., Wu, J.Z., , The Effect of an Interfacial Layer on Electron Tunneling through Atomically-Thin Al2o3 Tunnel Barriers. *ACS Applied Materials & Interfaces* **2017,** *9*, 37468.

36. Wilt, J.; Goul, R.; Acharya, J.; Sakidja, R.; Wu, J. Z., In Situ Atomic Layer Deposition and Electron Tunneling Characterization of Monolayer Al2o3 on Fe for Magnetic Tunnel Junctions. *Aip Advances* **2018,** *8*.

37. Wilt, J.; Gong, Y.; Gong, M.; Su, F.; Xu, H.; Sakidja, R.; Elliot, A.; Lu, R.; Zhao, S.; Han, S.; Wu, J. Z., Atomically Thin Al2o3 Films for Tunnel Junctions. *Physical Review Applied* **2017,** *7*, 064022.

38. Matero, R.; Rahtu, A.; Ritala, M.; Leskelä, M.; Sajavaara, T., Effect of Water Dose on the Atomic Layer Deposition Rate of Oxide Thin Films. *Thin Solid Films* **2000,** *368*, 1-7.

39. Acharya, J.; Wilt, J.; Liu, B.; Wu, J., Probing the Dielectric Properties of Ultrathin Al/Al2o3/Al Trilayers Fabricated Using in Situ Sputtering and Atomic Layer Deposition. *ACS applied materials & interfaces* **2018,** *10*, 3112-3120.

40. Elliot, A. J.; Malek, G.; Wille, L.; Lu, R.; Han, S.; Wu, J. Z.; Talvacchio, J.; Lewis, R. M., Probing the Nucleation of in Atomic Layer Deposition on Aluminum for Ultrathin Tunneling Barriers in Josephson Junctions. *Applied Superconductivity, IEEE Transactions on* **2013,** *23*, 1101405-1101405.

41. Elliot, A. J.; Malek, G. A.; Lu, R.; Han, S.; Yu, H.; Zhao, S.; Wu, J. Z., Integrating Atomic Layer Deposition and Ultra-High Vacuum Physical Vapor Deposition for in Situ Fabrication of Tunnel Junctions. *Review of Scientific Instruments* **2014,** *85*, 073904.

42. Ugeda, M. M.; Bradley, A. J.; Shi, S.-F.; Felipe, H.; Zhang, Y.; Qiu, D. Y.; Ruan, W.; Mo, S.-K.; Hussain, Z.; Shen, Z.-X., Giant Bandgap Renormalization and Excitonic Effects in a Monolayer Transition Metal Dichalcogenide Semiconductor. *Nature materials* **2014,** *13*, 1091-1095.

43. Feenstra, R. M.; Gaan, S.; Meyer, G.; Rieder, K., Low-Temperature Tunneling Spectroscopy of Ge (111) C (2× 8) Surfaces. *Physical Review B* **2005,** *71*, 125316.

44. Dorneles, L.; Schaefer, D.; Carara, M.; Schelp, L., The Use of Simmons' Equation to Quantify the Insulating Barrier Parameters in Al/Alo X/Al Tunnel Junctions. *Applied physics letters* **2003,** *82*, 2832-2834.

45. Wolf, C.; Köhler, U., Growth and Intermixing of Nb on Fe (110) and Fe on Nb (110). *Thin solid films* **2006,** *500*, 347-355.

46. Süle, P.; Kaptás, D.; Bujdosó, L.; Horváth, Z. E.; Nakanishi, A.; Balogh, J., Chemical Mixing at "Al on Fe" and "Fe on Al" Interfaces. *Journal of Applied Physics* **2015,** *118*, 135305.

47. Lu, R.; Elliot, A. J.; Wille, L.; Mao, B.; Han, S.; Wu, J. Z.; Talvacchio, J.; Schulze, H. M.; Lewis, R. M.; Ewing, D. J., Fabrication of Nb/Al2O3/Nb Josephson Junctions Using in Situ Magnetron Sputtering and Atomic Layer Deposition. *IEEE transactions on applied superconductivity* **2012,** *23*, 1100705-1100705.

48. Ventura, J.; Teixeira, J.; Araujo, J.; Sousa, J.; Ferreira, R.; Freitas, P.; Langer, J.; Ocker, B.; Maass, W., Influence of Pinholes on Mgo-Tunnel Junction Barrier Parameters Obtained from Current–Voltage Characteristics. *Journal of nanoscience and nanotechnology* **2010,** *10*, 2731-2734.

49. Wei, H. X.; Qin, Q. H.; Ma, M.; Sharif, R.; Han, X. F., 80% Tunneling Magnetoresistance at Room Temperature for Thin Al–O Barrier Magnetic Tunnel Junction with Cofeb as Free and Reference Layers. *Journal of Applied Physics* **2007,** *101*, 09B501.

50. Zhang, S.; Levy, P.; Marley, A.; Parkin, S., Quenching of Magnetoresistance by Hot Electrons in Magnetic Tunnel Junctions. *Physical Review Letters* **1997,** *79*, 3744.

51. Han, X.-F.; Andrew, C.; Oogane, M.; Murai, J.; Daibou, T.; Miyazaki, T., Analyses of Intrinsic Magnetoelectric Properties in Spin-Valve-Type Tunnel Junctions with High Magnetoresistance and Low Resistance. *Physical Review B* **2001,** *63*, 224404.

52. Aref, T.; Averin, A.; van Dijken, S.; Ferring, A.; Koberidze, M.; Maisi, V.; Nguyend, H.; Nieminen, R. M.; Pekola, J. P.; Yao, L., Characterization of Aluminum Oxide Tunnel Barriers by Combining Transport Measurements and Transmission Electron Microscopy Imaging. *Journal of Applied Physics* **2014,** *116*, 073702.

53. Zeng, L.; Nik, S.; Greibe, T.; Krantz, P.; Wilson, C.; Delsing, P.; Olsson, E., Direct Observation of the Thickness Distribution of Ultra Thin Alo X Barriers in Al/Alo X/Al Josephson Junctions. *Journal of Physics D: Applied Physics* **2015,** *48*, 395308.

54. Xu, X. D.; Mukaiyama, K.; Kasai, S.; Ohkubo, T.; Hono, K., Impact of Boron Diffusion at Mgo Grain Boundaries on Magneto-Transport Properties of Mgo/Cofeb/W Magnetic Tunnel Junctions. *Acta Materialia* **2018,** *161*, 360-366.

55. Teixeira, J. M.; Ventura, J.; Araujo, J. P.; Sousa, J. B.; Wisniowski, P.; Cardoso, S.; Freitas, P. P., Resonant Tunneling through Electronic Trapping States in Thin Mgo Magnetic Junctions. *Physical Review Letters* **2011,** *106*, 196601.

56. Zhu, J.-G.; Park, C., Magnetic Tunnel Junctions. *Materials Today* **2006,** *9*, 36-45.

57. Komagaki, K.; Hattori, M.; Noma, K.; Kanai, H.; Kobayashi, K.; Uehara, Y.; Tsunoda, M.; Takahashi, M., Influence of Diffused Boron into Mgo Barrier on Pinhole Creation in Cofeb/Mgo/Cofeb Magnetic Tunnel Junctions. *IEEE Transactions on Magnetics* **2009,** *45*, 3453-3456.

58. Bai, Z.; Shen, L.; Wu, Q.; Zeng, M.; Wang, J.-S.; Han, G.; Feng, Y. P., Boron Diffusion Induced Symmetry Reduction and Scattering in Cofeb/Mgo/Cofeb Magnetic Tunnel Junctions. *Physical Review B* **2013,** *87*, 014114.

59. Rumaiz, A. K.; Woicik, J. C.; Wang, W. G.; Jordan-Sweet, J.; Jaffari, G. H.; Ni, C.; Xiao, J. Q.; Chien, C. L., Effects of Annealing on the Local Structure of Fe and Co in Cofeb/Mgo/Cofeb Tunnel Junctions: An Extended X-Ray-Absorption Fine Structure Study. *Applied Physics Letters* **2010,** *96*, 112502.

60. Jang, Y.; Nam, C.; Lee, K.-S.; Cho, B.; Cho, Y.; Kim, K.-S.; Kim, K., Variation in the Properties of the Interface in a Co Fe B∕ Mg O∕ Co Fe B Tunnel Junction During Thermal Annealing. *Applied Physics Letters* **2007,** *91*, 102104.

61. Ke, Y.; Xia, K.; Guo, H., Oxygen-Vacancy-Induced Diffusive Scattering in Fe/Mgo/Fe Magnetic Tunnel Junctions. *Physical review letters* **2010,** *105*, 236801.

62. Martin, M.-B.; Dlubak, B.; Weatherup, R. S.; Yang, H.; Deranlot, C.; Bouzehouane, K.; Petroff, F.; Anane, A.; Hofmann, S.; Robertson, J., Sub-Nanometer Atomic Layer Deposition for Spintronics in Magnetic Tunnel Junctions Based on Graphene Spin-Filtering Membranes. *ACS nano* **2014,** *8*, 7890-7895.

63. Dlubak, B.; Martin, M.-B.; Weatherup, R. S.; Yang, H.; Deranlot, C.; Blume, R.; Schloegl, R.; Fert, A.; Anane, A.; Hofmann, S., Graphene-Passivated Nickel as an Oxidation-Resistant Electrode for Spintronics. *ACS nano* **2012,** *6*, 10930-10934.

64. Ryu, S. W.; Song, J.-G.; Kim, H. G.; Kim, H.; Lee, H.-B.-R., Interlayer-Assisted Atomic Layer Deposition of Mgo as a Magnetic Tunneling Junction Insulators. *Journal of Alloys and Compounds* **2018,** *747*, 505-510.

65. Gloos, K.; Koppinen, P.; Pekola, J., Properties of Native Ultrathin Aluminium Oxide Tunnel Barriers. *Journal of Physics: Condensed Matter* **2003,** *15*, 1733.

Table of content graphics:

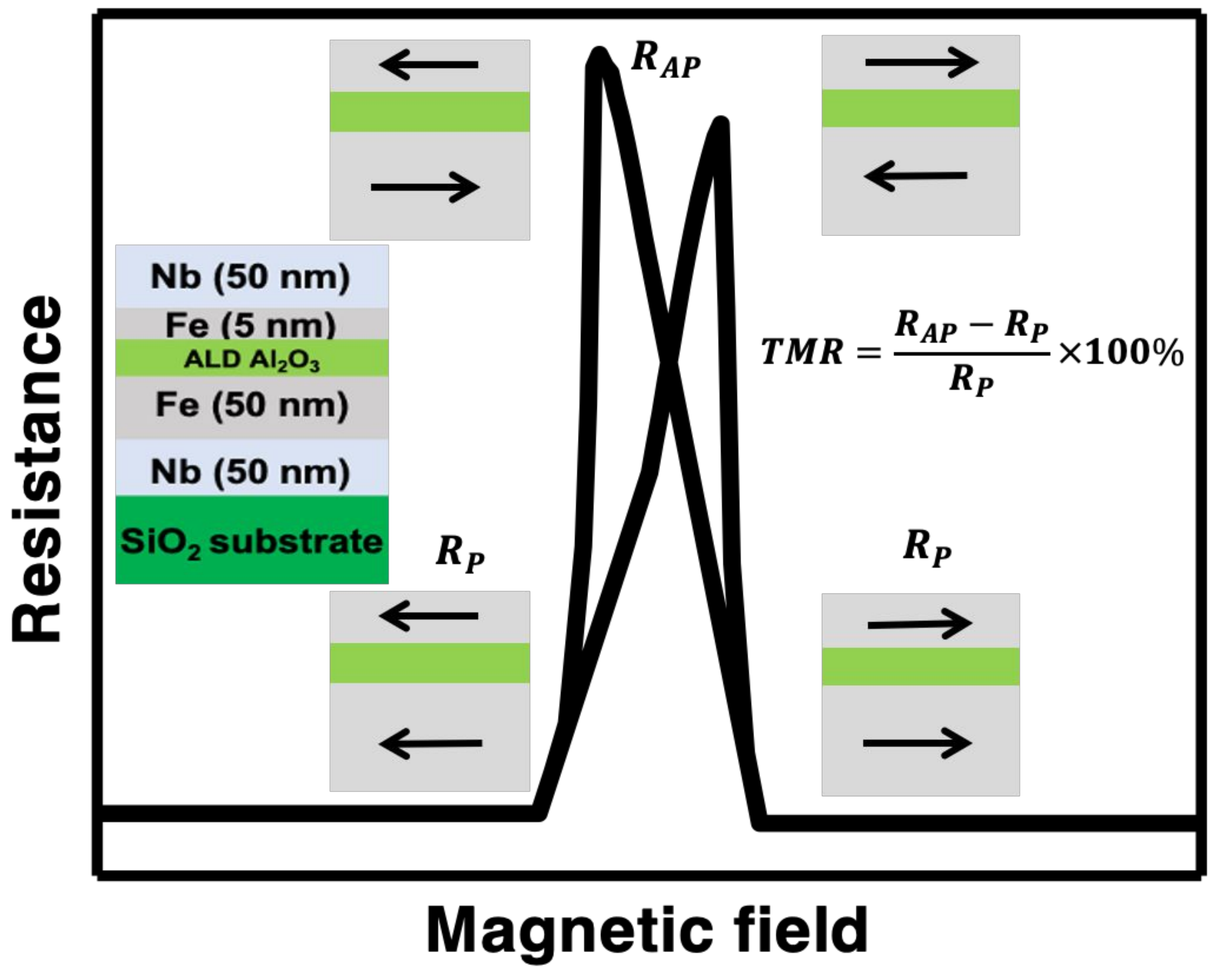
Resistance
Magnetic field
R_{AP}
Nb (50 nm)
Fe (5 nm)
ALD Al_2O_3
Fe (50 nm)
Nb (50 nm)
SiO_2 substrate
$TMR = \frac{R_{AP} - R_P}{R_P} \times 100\%$
R_P
R_P

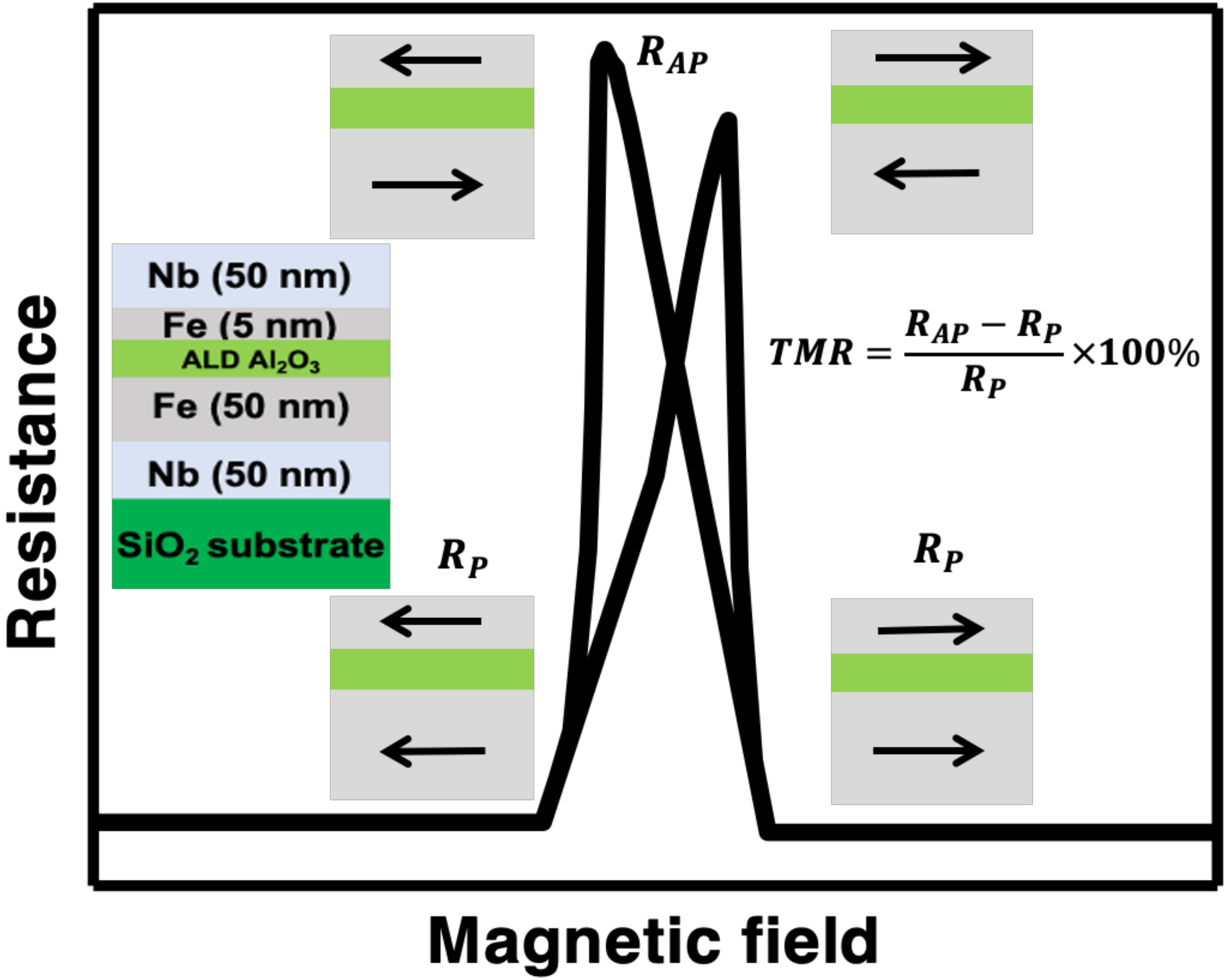
R_AP
Nb (50 nm)
Fe (5 nm)
ALD Al2O3
Fe (50 nm)
Nb (50 nm)
SiO2 substrate
R_P
R_P
TMR = (R_AP − R_P) / R_P ×100%
Resistance
Magnetic field